Nuclear Science and Techniques (2025) 36:190
https://doi.org/10.1007/s41365-025-01770-9

Saturation effect study and ion recombination correction on ionization chamber for ultra-high dose rate (FLASH) of carbon ions

Xin-Le Lang[1,2] · Zheng-Guo Hu[1,2] · Zhi-Guo Xu[1,2] · Juan Li[1] · Kai Zhou[1,2] · Fa-Ming Luo[1,2] · Yu-Cong Chen[1] · Rui-Shi Mao[1,2] · Chuan Huang[1] · Zu-Long Zhao[1] · Jia-Li Fu[1,2] · Li-Bin Zhou[1,2] · Guo-Qing Xiao[1,2]

Received: 9 July 2024 / Revised: 2 December 2024 / Accepted: 9 January 2025 / Published online: 24 July 2025

Abstract
The ionization chamber produces significant space-charge and ion recombination effects at ultra-high dose rates, posing a challenge for dose monitoring. In addition, there is no generally accepted ion correction model for dosimetry in FLASH radiotherapy, making it crucial to monitor the dose at ultra-high dose rates accurately and in real time. In this study, the air pressure of the ionization chamber was reduced to perform real-time beam monitoring, and a Faraday cup was used for calibration for active dosimetry. To study the saturation effect of the ionization chamber, the drift, attachment, recombination, and diffusion processes of the electron-ion pairs were modeled using finite-element analysis based on physical phenomenological principles, and the correction factor was calculated. The experimental results showed that the FLASH ionization chamber measures good dose linearity at a dose rate of approximately 0.2 Gy/s. When the air pressure of the chamber was adjusted to 10 mbar, the response of the FLASH ionization chamber was linear at a dose rate of approximately 50 Gy/s, with the residuals within 2%. Furthermore, by using physical phenomenology to resolve the process of electron-ion pair motion in the sensitive volume of the ionization chamber, the analytical model better describes the saturation effect of carbon ions at ultra-high dose rates. The maximum deviation in the calculated correction factor is less than 10%. We studied the saturation effect in dose measurement, achieving accurate and fast dose and profile position measurement across different dose rates in a wide range based on the Heavy Ion Research Facility in Lanzhou.

Keywords FLASH radiotherapy · Ultra-high dose rate · Carbon ions · Dosimetry · Saturation effect · Correction factor

1 Introduction

FLASH radiotherapy (RT) is a new technology that delivers radiation at ultra-high dose rates at orders of magnitude higher than those of conventional clinical RT [1, 2]. Recent results from preclinical studies with electron [3], photon [4–6], and proton [7–11] beams have shown that compared to conventional RT, FLASH RT can achieve similar tumor control while protecting normal tissues, which greatly increases the therapeutic window. However, for carbon ions, only a few laboratories can conduct these experiments. Compared with commercial proton RT instruments based on cyclotrons [12], heavy-ion accelerator technology has been greatly restricted [13, 14]. Because all currently operating carbon-ion treatment facilities use compact synchrotrons, they cannot satisfy the dose rate requirements for FLASH treatment [15–17]. However, the protective mechanisms of FLASH RT remain unclear. Many studies have reported that the FLASH effect needs to be characterized not only by the average dose rate but also by the beam delivery parameters [18]. Therefore, accurate and fast beam monitoring and dosimetric determination are crucial for the potential clinical benefits of this new technology and the promotion of its clinical transformation [19–21]. Dosimetric protocols such as those proposed by the IAEA [22] and AAPM [23] recommend an ionization chamber (IC) for the reference dosimetry of therapeutic photons, electrons, protons, and

✉ Zheng-Guo Hu
huzg@impcas.ac.cn

✉ Rui-Shi Mao
maorsh@impcas.ac.cn

[1] Institute of Modern Physics, Chinese Academy of Sciences, 730000 Lanzhou, China

[2] School of Nuclear Science and Technology, University of Chinese Academy of Sciences, 100049 Beijing, China

heavy-ion beams [24]. However, the ion recombination and space-charge effects in ICs have been widely investigated using FLASH RT dosimetry [25].

This is mainly due to the fact that the dose per pulse of the photon beam generated by flattening filter-free linear accelerators increases by approximately 0.8 mGy, and the electron beam used in the operation increases by 3–130 mGy, compared to the conventional photon beam generated by flat filter linear accelerators, which increases by approximately 0.3 mGy. In particular, the dose per pulse of FLASH RT increases by approximately 10–5000 mGy and requires the release of a large amount of dose in a very short time. Typically, the dose rate needs to be higher than 40 Gy/s.

The charge released in the IC is related to the absorbed dose. However, because of ion recombination, attachment, diffusion, and space-charge effects, the charge collected at the collector electrode is smaller than the charge released in the IC. In particular, at the ultra-high dose rate of FLASH RT, a significant ion recombination effect is observed in the IC, and there is a large deviation in the direct application of the current standard protocol. In addition, to use the IC as a reference dosimeter at ultra-high dose rates, the effect of ion recombination must be reconsidered. Ion recombination is a complex phenomenon that depends on detector characteristics and several properties of the beam, including linear energy transfer (LET), particle type, mode of radiation (continuous, pulsed, or pulsed-swept), and fluence rate. Different theoretical models have been used to describe the collection efficiency in parallel-plate ICs for the two main types of recombination: initial and volume recombination. The initial ionization occurs between the ions created in the same ionization track. This is an independent phenomenon of the ionization current but depends on the ionization density within the track. The second is volume recombination, which occurs between ions originating from different ionization tracks and depends on the ionization current. Consequently, this depends on the beam fluence rate.

For heavy-ion therapy, especially for carbon ions with high LET, both initial and volume recombination have a negative impact on dose measurement. Different theoretical models have been used to describe the dose measurement deviation caused by the saturation effect of ion recombination in the IC. The *Jaffe* method cannot adequately describe the recombination effect of heavy ions at ultra-high dose rates. It has been proven that the two-voltage method is not suitable for dose-correction calculations for heavy ions. The *Niatel* model can describe both initial recombination and volume recombination; however, it depends on experimental data to determine the fitting parameters, and there is no experiment to prove that it can describe the saturation effect of carbon ions in the case of FLASH irradiation.

Boag et al. [26] assumed that before the formation of a uniform negative ion cloud, the moving distance of free electrons released in the chamber volume could be neglected, whereas the negative ion cloud drifted slowly through the uniform positive ion cloud, and the positive ion cloud moved in the opposite direction. However, in 1996, Boag et al. [27] used the probability e^{-ad} of free electrons drifting d or longer in air before being attached to electronegative gas molecules. Immediately after a charged particle ionizes the medium between electrodes, there are no negative ions. Free electrons are collected at the anode, while the remainder form negative ions. Negative ions are then formed by the diffusion, drift, and attachment of free electrons to negatively charged gas molecules. The proportion of all the electrons that are not connected to the molecule is the free electron p, which is expressed by Eq. (1) [27]. Accordingly,

$$p = \frac{1}{nd}\int_0^d ne^{-ax}\mathrm{d}x = \frac{1}{ad}(1 - e^{-ad}) \tag{1}$$

where n is the initial concentration of positive ions following the pulse, d is the electrode spacing in a plane-parallel IC, and a, in units of inverse length, is a coefficient whose inherent properties depend on gas parameters, electric field strength, and sensitive volume of the air-filled IC, as derived by Thomson [28].

$$n_{-}(x, t = 0) = n_0(1 - \exp(-ax)) \tag{2}$$

In Eq. (2), n_0 is the uniform number density of positive ions (or electrons) initially released by the radiation pulse, x is the distance to the cathode, and $t = 0$ indicates the early time before the significant movement of ions [27, 29].

When positive and negative ions (including electrons) drift uniformly toward each other, the total number of ion recombinations can be calculated directly because the ion recombination rate generated in the entire overlap region is also uniform [27]. When the negatively charged cloud is initially non-uniform, the ion recombination rate changes throughout the overlap, causing the positive ion cloud to become non-uniform and making the number of recombinations more difficult to determine. Boag et al. [27] provided three approximate formulas, f''', f'', and f', for the collection efficiency of the IC, defined as the ratio of the charge collected by the IC to the charge released in its sensitive volume. The reciprocal is called the correction factor and is generally expressed in k_s. These equations (3–5) are based on three uniform approximations of the non-uniform initial negative ion density of Eq. (2):

$$f' = \frac{1}{u}\ln\left(1 + \frac{e^{pu} - 1}{p}\right), \tag{3}$$

$$f'' = p + \frac{1}{u}\ln(1 + (1 - p)u), \tag{4}$$

$$f''' = \lambda + \frac{1}{u}\ln\left(1 + \frac{e^{\lambda(1-\lambda)u} - 1}{\lambda}\right), \tag{5}$$

$$u = \frac{\alpha}{\mu_+ + \mu_-}\frac{n_+ d^2}{V}, \lambda - 1 - \sqrt{1-p}. \tag{6}$$

Boag et al. [27] predicted that f''' is more accurate than f'', and f'' is more accurate than f' because the approximations f''', f'' and f' in theory seem to provide a step-by-step improved method description of the exponential change of ion density with d. In most cases, all three formulas are used to calculate the correction factor (collection efficiency), and f' is calculated separately because of the nature of the formula itself [30].

However, Boag et al. [27] did not express a specific preference for adopting any of these three models under the given experimental conditions. Therefore, they recommended further investigation. Moreover, there is no systematic and comprehensive interpretation of the method and numerical calculation process for reducing ion recombination and space-charge effects in dose measurements under ultra-high dose rates. It has been proven that there is a large deviation at ultra-high dose rates. However, these models cannot accurately estimate the ion recombination correction factors. The lack of a generally accepted model for ultra-high dose rates to accurately measure the dose across a wide range of dose rates and doses remains an issue, especially in FLASH RT studies.

Therefore, in this study, we established a beam-monitoring and dose measurement system to meet the requirements of carbon-ion FLASH preclinical experiments based on the Heavy Ion Research Facility in Lanzhou (HIRFL). Real-time online dose measurements and beam profile distributions were obtained by reducing the air pressure in the IC. The saturation effect was studied by varying the applied voltage in the FLASH IC. Under different beam currents (dose rates), considering the space-charge, ion recombination, attachment, and diffusion effects in the process of carrier movement in the sensitive volume, a model was established based on physical phenomenology, and the correction factors were calculated using finite-element analysis. At the same time, the experimental data were used as the standard to verify and analyze them. This study aims to identify key technical problems and solutions for carbon-ion FLASH projects. Therefore, these detailed dosimetric parameters provide a methodological basis for preclinical FLASH experiments and play a crucial role in providing machine support for the study of carbon-ion FLASH-related mechanisms.

2 Materials and methods

2.1 Irradiation terminal and beam line control system of accelerator

Figure 1a shows the passive beam delivery system installed on the shallow-seated (80.55 MeV/n carbon ions) FLASH irradiation terminal of the HIRFL. Because the accelerator can provide a constant beam current, the scanning magnet deflects the pencil beam quickly and continuously in a zigzag scanning manner to achieve transverse beam diffusion and generate a larger radiation field [31]. The X and Y directions are high- and low-frequency zigzag periodic current-driven magnets that control the target volume of irradiation by adjusting different frequencies in the X and Y directions. Thus, the magnetic scanning system guides the focused beam to draw the target volume at the center of the treatment terminal in a Lissajous or raster-like pattern depending on the difference between the fast and slow frequencies. The terminal monitoring system consisted of three large-area penetrating ICs (Fig. 1a): a dose IC, an integrated dose-position monitoring FLASH IC, and a position monitoring IC. The output signal of the FLASH IC was directly connected to the FEMTO variable-gain low-noise amplifier for I/V conversion, and a small current was directly converted into the available voltage. The data acquisition system was based on a National Instruments (NI) cRIO 9063 with a real-time operating system and an NI 9215 analog input card to achieve rapid acquisition. During the irradiation process, when the dose measured by the dose IC reached a set value, the automatic sample-change system changed to the next sample. If the position IC monitors that the beam profile uniformity does not meet the experimental requirements, the irradiation of the interlocking system is stopped [32, 33].

Through the chopper system, a pulse beam was generated and cut off, and the response accuracy reached the nanosecond level to satisfy the FLASH irradiation requirements. The beam-time structure adjusts the signal characteristics to excite the pulse generator by setting parameters such as the frequency, amplitude, and duty cycle of the pulse through the signal generator. The direct-current (DC) voltage generated by the high-voltage DC power supply enters the pulse generator and is modulated by the transistor–transistor logic gate signal generated by the signal generator. The output voltage of the high-voltage power supply was compared with the set reference voltage. When the difference between the two reaches a specified threshold, the counter triggers the output pulse signal, and its output is loaded onto the ion source extraction electrode. When the carbon-ion beam is extracted, pulse modulation

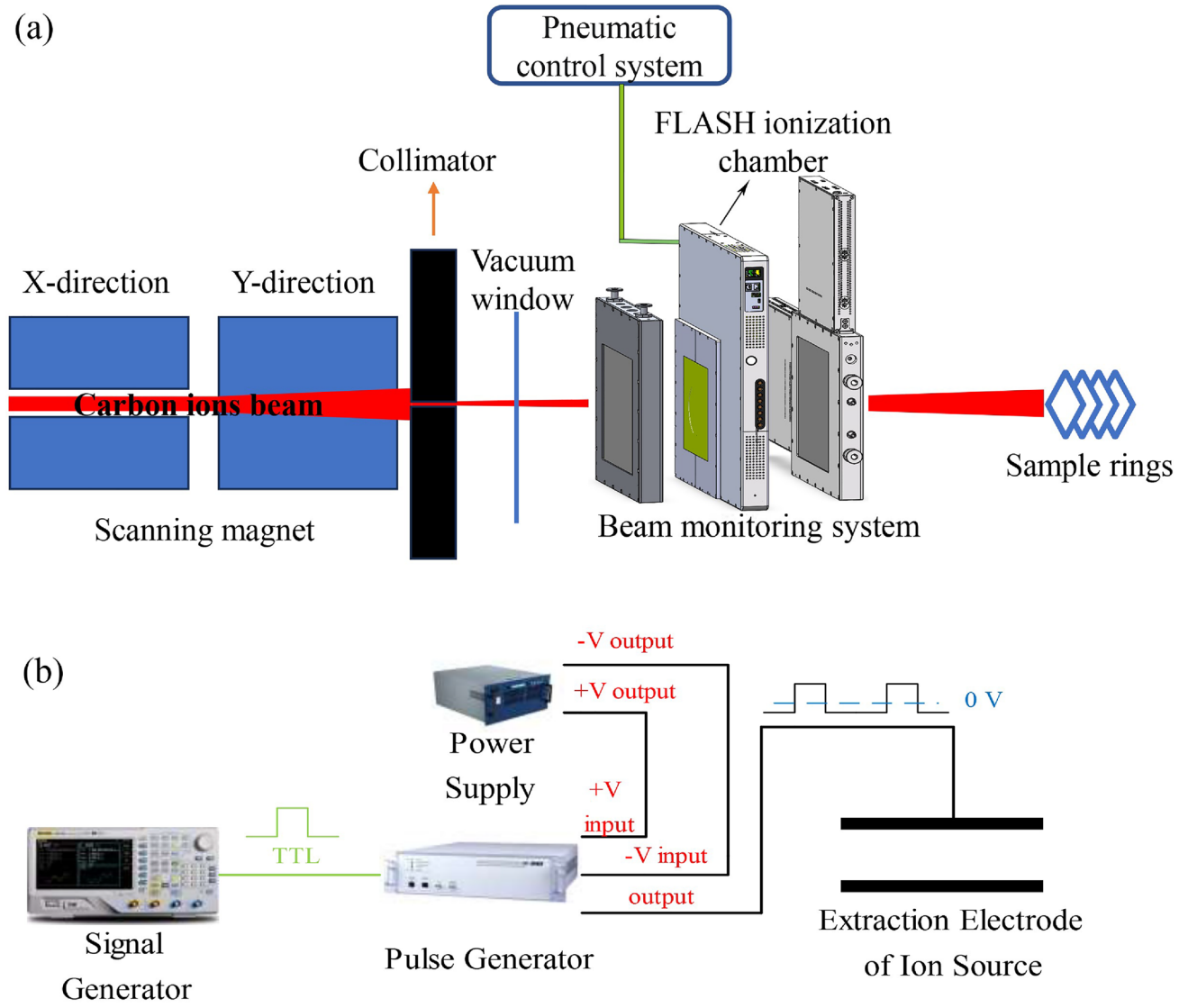

Fig. 1 (Color online) FLASH shallow-seated irradiation terminal beam monitoring and dose measurement schematic at HIRFL (**a**). Schematic of the generation of a pulse beam (**b**)

of the carbon-ion beam current is achieved. A schematic of this process is shown in Fig. 1b.

2.2 Physical process analysis

The FLASH IC is based on a parallel-plate IC. The chamber can be simplified as a high-voltage electrode, gas gap, and collection-signal electrode. The air gap thickness was 4 mm. Air was used as the working gas in the experiments. During the experiment, the entire sensitive volume was ensured to have a uniform electric field in the FLASH IC. Simultaneously, there is a high line-energy transfer of the radiation mass, such as carbon ions. We should consider not only volume recombination but also initial recombination based on the amorphous track structure theory [34, 35].

To this end, the following four-step procedure was implemented: (1) Electrons and cations are generated according to the intensity distribution of the ion beam and the resulting ionization density between the two electrodes with a gap size of d. (2) The corresponding charge is recombined according to the coefficients (recombination, attachment, and diffusion coefficients). (3) The electric field in the sensitive volume of the FLASH IC was calculated, and the superposition of the external electric field caused by the applied voltage and the internal electric field generated by the charge carrier was calculated. (4) The electron-ion pair drifts with the calculated electric field.

In the experiment, the particle current density $\vec{J}_{\pm}$ of the positive and negative ions is in units of charge carriers per unit area per unit time, which consists of the contribution of drift

caused by the electric field $\vec{E}$ and diffusion $D_{\pm}$ caused by the concentration gradient, and is given as

$$\vec{J}_{\pm}(\vec{r},t) = -D_{\pm}\nabla\rho_{\pm}(\vec{r},t) \pm \frac{p_0}{p}\vec{E}\mu_{\pm}\rho_{\pm}(\vec{r},t), \tag{7}$$

where $n_{\pm}$ is the charge carrier density and $\mu_{\pm}$ is the mobility of the positive and negative ions. We introduced ion recombination and attachment coefficients into the continuous equation as follows:

$$\frac{\partial\rho_{\pm}(\vec{r},t)}{\partial t} + \vec{\nabla}\cdot\vec{J}_{\pm} = -\alpha\rho_{+}(\vec{r},t)\rho(\vec{r},t) \pm \gamma\rho_{\mathrm{e}}. \tag{8}$$

Equation (8) can be written as

$$\frac{\partial\rho_{\pm}}{\partial t} = D_{\pm}\nabla^2\rho \mp \mu_{\pm}\frac{p_0}{p}\left(\vec{E}\cdot\vec{\nabla}\rho_{\pm} + \rho\vec{\nabla}\cdot\vec{E}\right) - \alpha\rho_{+}\rho_{-} \pm \gamma\rho_{\mathrm{e}}. \tag{9}$$

$\mu_{\pm}\frac{p_0}{p}\vec{E}\cdot\vec{\nabla}\rho_{\pm}$ is expressed in units of charge carriers per unit sensitive volume per unit time, and $\mu_{\pm}\frac{p_0}{p}\rho\vec{\nabla}\cdot\vec{E}$ represents the change in ion drift velocity caused by the space-charge effect in the sensitive volume. The space-charge effect shields the charge carriers released from the external electric field and causes the observed charge carriers (electron-ion pairs) to change the drift velocity to the opposite polarity electrode. This effect is very obvious at ultra-high dose rates. To simulate the ion transport process of the sensitive volume in the FLASH IC at an ultra-high dose rate, Eqs. (10)–(12) are used to describe the physical process of charge carriers. In our model, we considered three types of carriers (positive ions, negative ions, and electrons) for formation, interaction, and motion in the FLASH IC. The evolution equations describing the time-dependent processes of various carriers can be obtained as follows:

$$\begin{aligned}\frac{\partial\rho_{+}}{\partial_t} = {} & +R(t) - \frac{\alpha}{e}\rho_{+}\rho_{-} - \frac{\beta}{e}\rho_{+}\rho_{\mathrm{e}} - D_{+}\nabla^2\rho_{+} \\ & -\mu_{+}\frac{p_0}{p}\vec{E}\cdot\vec{\nabla}\rho_{+} + \mu_{+}\frac{p_0}{p}\rho_{+}\vec{\nabla}\cdot\vec{E}\end{aligned} \tag{10}$$

$$\begin{aligned}\frac{\partial\rho_{-}}{\partial_t} = {} & +\gamma\rho_{\mathrm{e}} - \frac{\alpha}{e}\rho_{+}\rho_{-} - D_{-}\nabla^2\rho_{-} \\ & +\mu_{-}\frac{p_0}{p}\vec{E}\cdot\vec{\nabla}\rho_{-} - \mu_{-}\frac{p_0}{p}\rho_{-}\vec{\nabla}\cdot\vec{E}\end{aligned} \tag{11}$$

$$\begin{aligned}\frac{\partial\rho_{\mathrm{e}}}{\partial_t} = {} & +R(t) - \gamma\rho_{\mathrm{e}} - \frac{\beta}{e}\rho_{+}\rho_{\mathrm{e}} - D_{\mathrm{e}}\nabla^2\rho_{e} \\ & +\mu_{\mathrm{e}}\frac{p_0}{p}\vec{E}\cdot\vec{\nabla}\rho_{\mathrm{e}} - \mu_{\mathrm{e}}\frac{p_0}{p}\rho_{\mathrm{e}}\vec{\nabla}\cdot\vec{E}\end{aligned} \tag{12}$$

$R(t)$ is the charge production rate due to irradiation, and $\rho_i (i = +, -, e)$ are the positive, negative, and electron densities, respectively. $\gamma\rho_{\mathrm{e}}$ is the contribution rate of the electron attachment. α is the positive and negative ion recombination coefficient, and β is the positive ion and electron recombination coefficient. μ_i denotes the mobility of species i , , $\vec{E}$ denotes the electric field strength, and P/P_0 is the standard air pressure in units of air pressure. The electric field dependence of the chamber due to the space-charge effect can be calculated by solving the following one-dimensional Poisson equation:

$$\frac{\partial E(x,t)}{\partial x} = \frac{e}{\epsilon}\left[\rho_{+}(x,t) - \rho_{-}(x,t) - \rho_{\mathrm{e}}(x,t)\right] \tag{13}$$

where ϵ is the medium's dielectric constant.

2.3 The finite-element method

The above equations (10–12) are coupled with the partial differential equations without analytical solutions. Therefore, we can obtain the numerical solutions by converting them into ordinary differential equations using a first-order upwind technique, as shown in Eq. 15. To this end, the spatial derivative is first used to discretize the term, which produces an ordinary differential equation set (only the time derivative remains). The obtained system can then be integrated numerically [36]. The specific finite-element analysis method is introduced as follows:

The k_{s} values for the ion recombination and space-charge shielding effects were calculated. Equations (10)–(12) were solved using the finite-element method. The spatial first-order upwind technique was used to implement discretization in Equation (15), and the forward Euler method was used for time integration in Eqs. (20)–(21). For the numerical solution, the sensitive volume perpendicular to the electrode direction was divided into N bins of size h and two bins outside the sensitive volume (Fig. 2). The standard advection–diffusion reaction model deals with the time evolution of species in a flowing medium such as water or air. The mathematical equations describing this evolution are partial differential equations derived from mass balances. If $\bar{\rho}(x,t)$ is uniform, then $t \geq 0$ and $0 < h < D_{\mathrm{p}}$, and in $\left[x - \frac{1}{2}h,\ x + \frac{1}{2}h\right]$

$$\begin{aligned}\bar{\rho}(x,t) &= \frac{1}{h}\int_{x-\frac{1}{2}h}^{x+\frac{1}{2}h}\rho(s,t)\mathrm{d}s \\ &= \rho(x,t) + \frac{1}{24}h^2\frac{\partial^2}{\partial x^2}\rho(x,t) + \cdots\end{aligned} \tag{14}$$

The model conditions satisfy the law of conservation of mass; therefore, the change in $\bar{u}(x,t)$ per unit time is the net balance of the inflow and outflow over the bin boundaries.

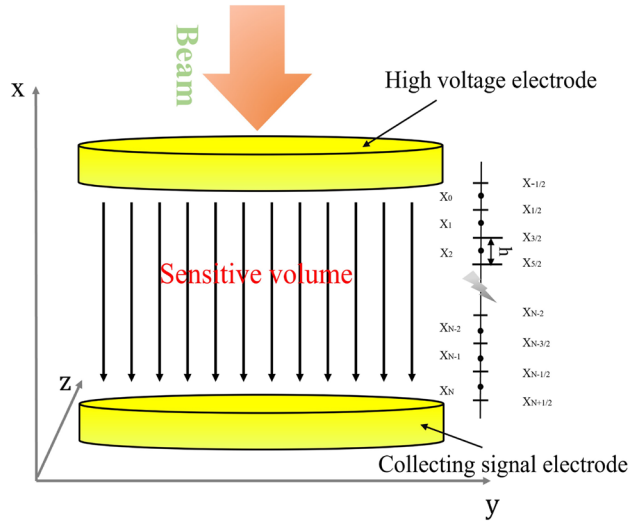

Fig. 2 (Color online) Discrete internal schematic of the sensitive volume of the flat IC, where X_0,..., X_N are the main grid points, and $X_{-\frac{1}{2}}$, ..., $X_{N+\frac{1}{2}}$ are auxiliary grid points. Concentration is defined at the main grid points and can be regarded as the average value of the entire unit, while electric field intensity and related input parameters are calculated at the unit boundary

$$\frac{\partial}{\partial t}\rho(x,t) = \frac{1}{h}\left[v\left(x-\frac{1}{2}h,t\right)\rho\left(x-\frac{1}{2}h,t\right) - v\left(x+\frac{1}{2}h,t\right)\rho\left(x+\frac{1}{2}h,t\right)\right] \tag{15}$$

where $v\left(x \mp \frac{1}{2}h,t\right)\rho\left(x \mp \frac{1}{2}h,t\right)$ denotes the mass flux over the left and right bin boundaries. Therefore, the advection equation can be written as follows:

$$\frac{\partial}{\partial t}\rho(x,t) + \frac{\partial}{\partial x}(v(x,t)\rho(x,t)) = 0 \tag{16}$$

We considered the effects of diffusion in the same manner.

$$\frac{\partial}{\partial t}\rho(x,t) = \frac{\partial}{\partial x}\left(D(x,t)\frac{\partial}{\partial x}\rho(x,t)\right) \tag{17}$$

There may also be a local change in $\rho(x,t)$ that is described by

$$\frac{\partial}{\partial t}\rho(x,t) = f(t,\rho(x,t)) \tag{18}$$

In summary, the advection–diffusion reaction equation is

$$\frac{\partial}{\partial t}\rho(x,t) + \frac{\partial}{\partial x}(v(x,t)\rho(x,t)) = \frac{\partial}{\partial x}\left(D(x,t)\frac{\partial}{\partial x}\rho(x,t)\right) + f(t,\rho(x,t)) \tag{19}$$

Therefore, the integral of each step is obtained as

$$\rho(t_i+\Delta t) - \rho(t_i) = \int_{t_i}^{t_i+\Delta t} f(t,\rho(t)\mathrm{d}t \approx \Delta t f(t_i,\rho(t_i)) \tag{20}$$

where $\triangle t \le \frac{h}{|v|}$, and the forward Euler method is used for the iterative calculation

$$\rho(t_{i+1}) = \rho(t_i) + \Delta t f(t_i,\rho(t_i)) \tag{21}$$

The first-order upwind technique was used for discretization, and the forward Euler method was used for step iteration. We attempt to require $h \longrightarrow 0$ and $\triangle t \longrightarrow 0$ to ensure that the calculation results converge more strictly to a real physical understanding. Therefore, the first-order upwind technique first takes the value of the upstream node directly on the boundary surface. Although the definition of upstream depends on the flow direction, the calculated flux is consistent. Therefore, the upwind scheme is conservative. The second condition is the boundary condition. The upwind scheme satisfies the Scarborough boundedness criterion. The coefficient matrix obtained after discretization is diagonally dominant; therefore, the numerical results do not exhibit an "oscillation" phenomenon, similar to the central difference scheme. However, false diffusion occurs when the number of grids is large. Grid encryption is often required to avoid this problem. The maximum upper limit of the bin size (h) was determined using the Einstein–Smoluchowski relation [37–39]

$$D_\mathrm{p} = \frac{\mu_\mathrm{e} k_\mathrm{B} T}{q} \tag{22}$$

where q is the particle charge, k_B is the Boltzmann constant, and T is the temperature. In addition, the physical diffusion must be greater than the numerical diffusion ($D_\mathrm{p} > D_\mathrm{n} = \frac{1}{2}hv$). Considering that $v = P_0/P\mu_\mathrm{e}E$ and that the electron has a charge $q = e$, the equation can be transformed into $h = 2k_\mathrm{B}T/(Ee)$, where $T = 300$ K and the pressure is the standard atmospheric pressure, that is, $P_0/P = 1$. It is evident that the first-order upwind scheme considers the directionality of the flow; thus, it has good transportability.

2.4 Parameters of the numerical solution

Air was used as the working gas in the experiment. The equation contains several physical parameters: recombination coefficient (α), electron attachment coefficient (γ), diffusion coefficient (D), and ion mobility (μ_i) (including positive ions, negative ions, and electrons). The electron drift velocity (Fig. 3a) and diffusion coefficient (Fig. 3c) under different electric field strengths were determined using the Garfield++ simulation. We used test data from Hochhäuser et al. [40] and Boissonnat et al. [41] for the spline interpolation to determine the electron attachment coefficient (Fig. 3b).

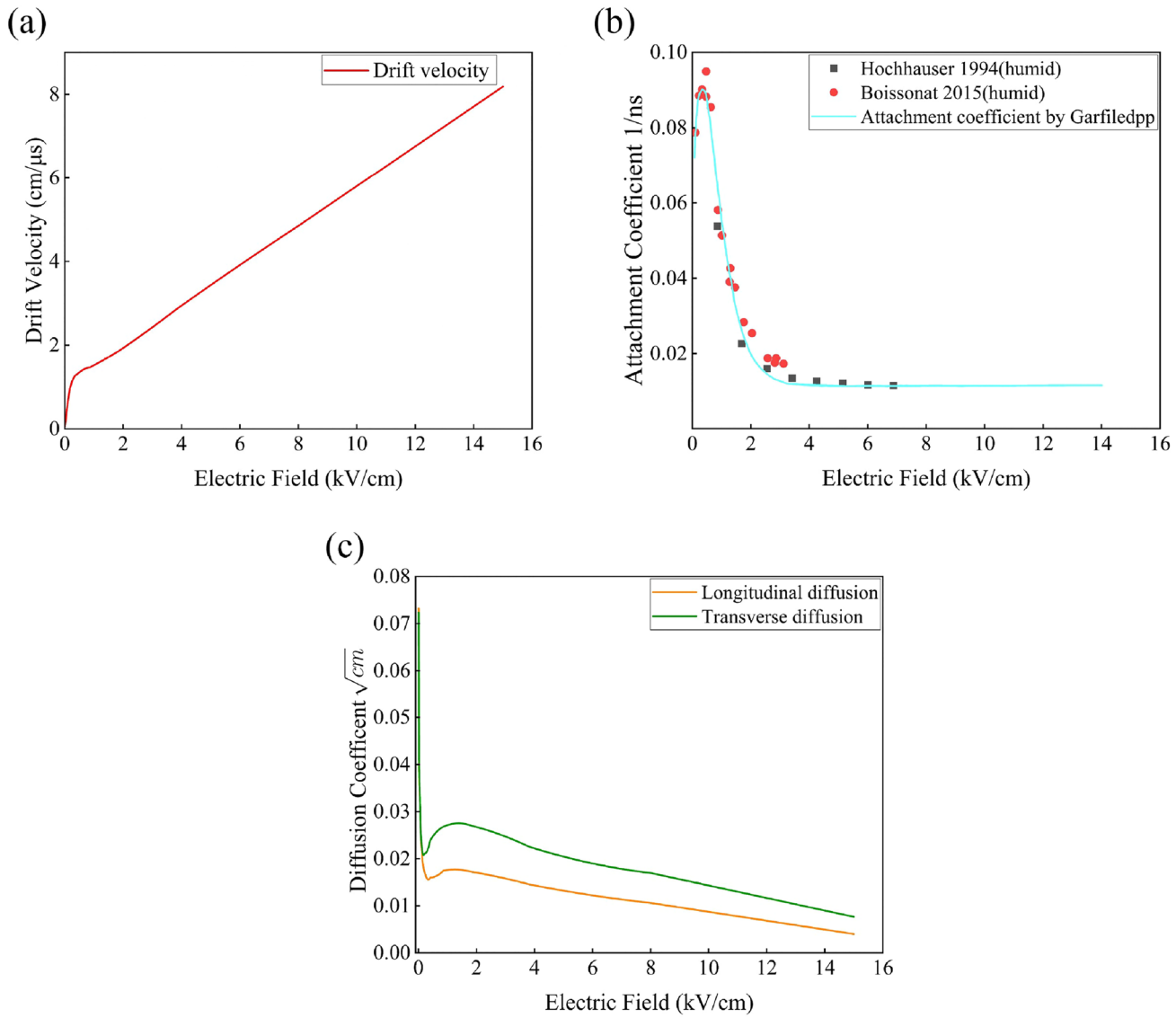

Fig. 3 Figure shows the electric field-dependent parameters used in the calculation. Figure (a) shows the electron drift velocity ($v = P_0/P\mu_e E$) by the Garfield++ simulation for humid air. Figure (b) shows the attachment coefficient (γ) of the electrons. The regression spline used in the numerical calculation is shown together with experimental data from Hochhäuser et al. [40] and Boissonnat [41] for humid air. Figure (c) shows the transverse and longitudinal diffusion coefficients (D_e) in different field strengths of electrons simulated by Garfield++ for humid air

Simultaneously, the positive and negative ion mobilities and diffusion coefficients were good approximation constants for the variation range of the electric field strength of the IC during the experiment. The specific parameters are listed in Table 1.

2.5 Experimental correction factor $k_{s\text{-}exp}$ determination

A Faraday cup was used to calibrate the reference dose of the FLASH IC. A relevant description is provided in Ref. [33]. The liberated charges $Q_0 = c \times (FC - FC_0)$, FC and

Table 1 Input relevant parameters in calculation model [27, 28, 42]

Constant	Symbol	Unit	Value
Positive ion diffusion	D_+	$cm^2\ s^{-1}$	2.82×10^{-2}
Negative ion diffusion	D_-	$cm^2\ s^{-1}$	4.35×10^{-2}
Positive ion mobility	μ_+	$cm^2\ V^{-1}\ s^{-1}$	1.36
Negative ion mobility	μ_-	$cm^2\ V^{-1}\ s^{-1}$	2.10
Recombination constant *(positive negative)*	α	$cm^3\ s^{-1}$	1.3×10^{-6}
Recombination constant *(positive electron)*	β	$cm^3\ s^{-1}$	0.4×10^{-6}

FC_0 are the signal and background of the Faraday cup, and c is the conversion factor. The measured charge of the IC is given by $Q_c = IC - IC_0$, where IC and IC_0 are the signal and background of the FLASH IC, respectively. Therefore, the correction factor k_s is expressed as follows:

$$k_{s\text{-exp}} = \frac{Q_0}{Q_c} = \frac{c \times (FC - FC_0)}{IC - IC_0} \tag{23}$$

The background of the FLASH IC and Faraday cup must be deducted before each measurement. According to physical theory, when $Q_0 = 0$, there must be $Q_c = 0$, which means that there is no recombination in the FLASH IC; therefore, $k_{s\text{-exp}} = 1$, which is of significant importance for dose measurement.

3 Results

3.1 Dose measurement and profile monitoring of ionization chamber under low pressure

The beam current of the terminal was tested using a Faraday cup to ensure that the PTW Roos-34001 IC was within the normal working range. The extrapolation of the Faraday cup measurements at an ultra-high dose rate (approximately 50 Gy/s) demonstrates that the beam current can fulfill the requirements of FLASH irradiation. Considering the experimental field environment, the carbon-ion beam current at an ultra-high dose rate was measured by reducing the air pressure of the chamber. The replacement of the working gas (such as helium) can alleviate ion recombination but cannot obtain completely satisfactory results at ultra-high dose rates. Considering the experimental environment within the field, the beam current at an ultra-high dose rate was measured by reducing the air pressure within the chamber. The replacement of the working gas (for example, helium) can mitigate ion recombination; however, the results obtained at an ultra-high dose rate are not entirely satisfactory. The large-area real-time beam-monitoring system for carbon-ion FLASH irradiation is susceptible to the effects of reduced electrode plate spacing, owing to the limitations of processing technology and the accuracy of the electrode plate. Additionally, this reduction is prone to a "light" phenomenon, which results in irreversible damage to the detector.

Figure 4(a) shows the dose measurement results of the FLASH IC at a dose rate of approximately 0.2 Gy/s under standard atmospheric pressure. The output of the PTW Roos-34001 IC was used as the reference dose. Figure 4(b) shows the dose residuals of the FLASH IC. Under the condition of IC pressure of 10 mbar and a dose rate of approximately 50 Gy/s, the dose linear curve (Fig. 4c) and residual diagram (Fig. 4d) of the FLASH IC were obtained. A Faraday cup was used to verify the reference dose of the FLASH IC. The results in Fig. 4 show that the IC can simultaneously meet the beam monitoring and dose measurement requirements of carbon-ion irradiation under conventional clinical and FLASH RT. The residuals were less than 2%, and as the dose increased, the deviation gradually decreased and approached 0%, which meets the requirements for preclinical dose monitoring.

Figure 5 shows that the beam spot was adjusted to approximately 40 mm in diameter, and the beam profile was measured using the FLASH IC and EBT3 films. Because the beam was defocused at the measurement position and the film was placed on the lower surface of the FLASH IC, the results for the film were slightly larger. The FLASH IC can measure the position profile of carbon-ion beams at ultra-high dose rates. During the experiment, the beam-scanning system was adjusted so that different volume targets at the isocenter could be irradiated.

3.2 Measuring saturation curve and calculating correction factor

Figure 6a shows that the ion recombination effect at different dose rates was tested by increasing the polarization voltage of the IC. The response of FLASH IC was characterized by a Faraday cup monitoring the beam current to obtain the saturation curve using Eq. (23). The results showed that the recombination effect of ions decreased with increasing polarization voltage. Theoretically, the voltage can be increased in the ionization region to obtain a linear dose curve. However, owing to the high polarization voltage applied at the ultra-high dose rate, the IC will be "light"; thus, the maximum polarization voltage is set to 400 V. Figure 6b shows the correction factor obtained by experimental calculation and model calculation. The results indicate that the correction factor calculated using the model is in good agreement with the experimental results. During the experiment, when a higher polarization voltage was applied, such as 200 or 400 V, the maximum deviation in the results was less than 5%. However, when the polarization voltages were 100 V and 50 V, the maximum deviation was less than 10%.

4 Discussion

At present, the shallow-seated carbon-ion FLASH treatment device based on HIRFL can realize subtle modulation of the beam current through chopper control technology and can arbitrarily change the pulse width and repetition frequency. From the perspective of treatment devices, this has been proven to be sufficient for preclinical experiments. To ensure that beam position profile monitoring and dose measurement can be carried out in real time during the irradiation

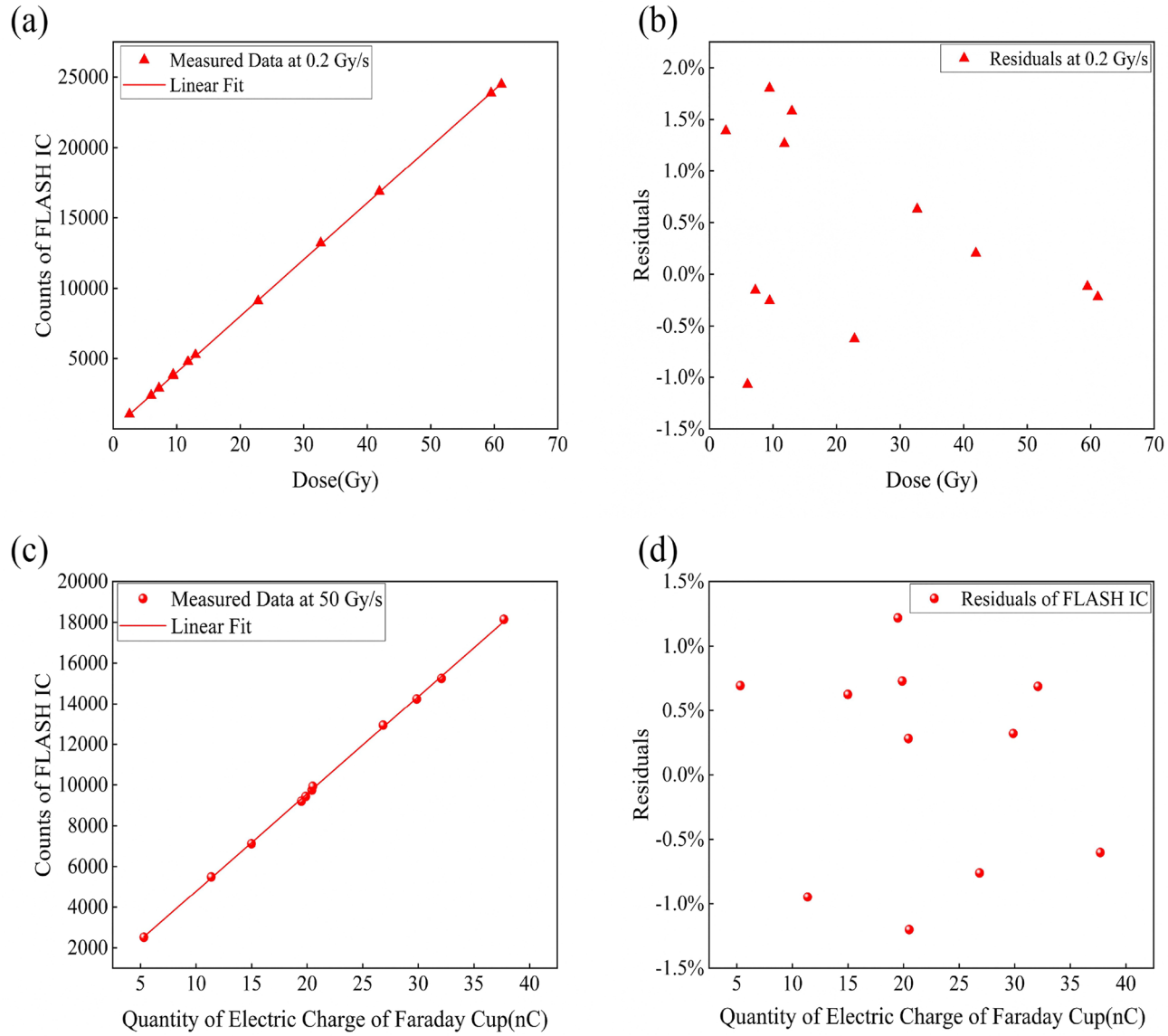

Fig. 4 Dose linear curve and residual diagram of FLASH IC at different pressures and dose rates

process, a large-area real-time monitoring FLASH IC and beam feedback control system with adjustable air pressure were designed.

Combined with previous work [33], Fig. 4(c) and (d) shows that the method of reducing the chamber air pressure can satisfy the FLASH irradiation dose measurement of carbon ions at ultra-high dose rates. The essential reason for this is that when the air pressure in the chamber is reduced, the number of gas molecules is significantly decreased, which reduces the generation of electron-ion pairs and the probability of collision with particles; thus, the saturation effect is eliminated. In addition, with a decrease in gas molecules, the attachment, ion recombination, and space-charge effects are significantly reduced, whereas the mobility is significantly increased, which positively impacts accurate dose measurement. The method proposed in this paper can meet beam monitoring and dose measurement requirements at different dose rates. We found that increasing the polarization voltage did not improve the saturation effect at ultra-high dose rates. Therefore, a finite-element analysis method based on the drift, diffusion, attachment, and recombination of electron-ion pairs was proposed to perform dose correction on the saturation curve. Additionally, the experimental data were compared. When the beam current measured using the Faraday cup was less than 4 nA, the model correction was in good agreement with the experimental calculation results, and the maximum deviation was less than 2%, satisfying

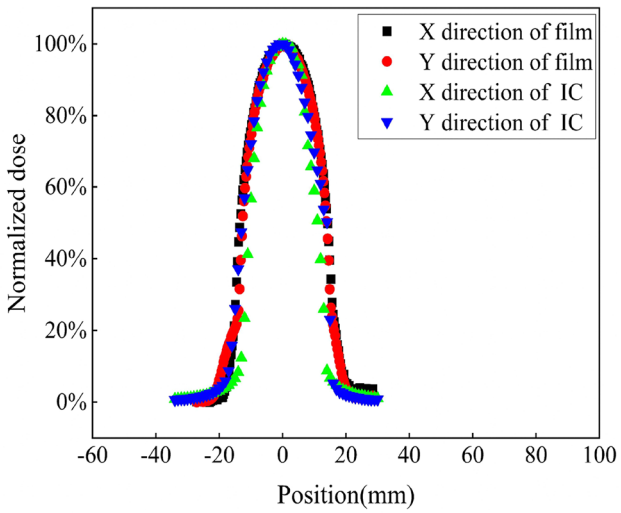

Fig. 5 (Color online) Beam profile position measurement of FLASH IC and EBT3 film at a dose rate of 50 Gy/s

the dose monitoring requirements of the FLASH irradiation process. When the beam current was greater than 4 nA, the space-charge effect was significantly enhanced, which distorted the applied electric field. Although the influence of the space-charge effect on the results was considered in the model, the recombination coefficient between ions is generally determined by a semi-empirical formula that combines the model and experimental data, which is a very complex physical and chemical process [43]. The recombination coefficient (α) in the numerical calculation model is a variable that makes it difficult to determine whether it is found in the actual measurements or in this study. In this study, no better calculation method for the recombination coefficient was found; therefore, the analysis was due to the deviation introduced by its uncertainty.

For real-time monitoring of large-area doses, we adopted a more effective method of reducing the pressure in the IC to avoid ion recombination and space-charge effects. This work begins with the working principle of the IC, combines physical phenomena to analyze the initial recombination and volume recombination of carbon ions with a relatively high LET, and verifies this through experiments. To eliminate the influence of the saturation effects introduced during dose measurement, it is possible to reduce the sensitive volume from the detector design to reduce the ion drift path and reduce the drift time or improve the polarization voltage to increase the drift speed. Using a working gas with a higher average ionization energy can reduce the production of electron-ion pairs. Alternatively, a combination of the aforementioned methods may be employed. However, from the perspective of physical theory, it is evident that no single method can effectively eliminate the saturation effect. Because FLASH RT increases the dose rate by nearly three orders of magnitude compared to conventional RT, reducing the pressure from atmospheric pressure to less than 10 mbar can meet its requirements, and for electron beam FLASH irradiation with extremely high dose rates ($>1\times10^5$ Gy/s), this method can meet the needs very well.

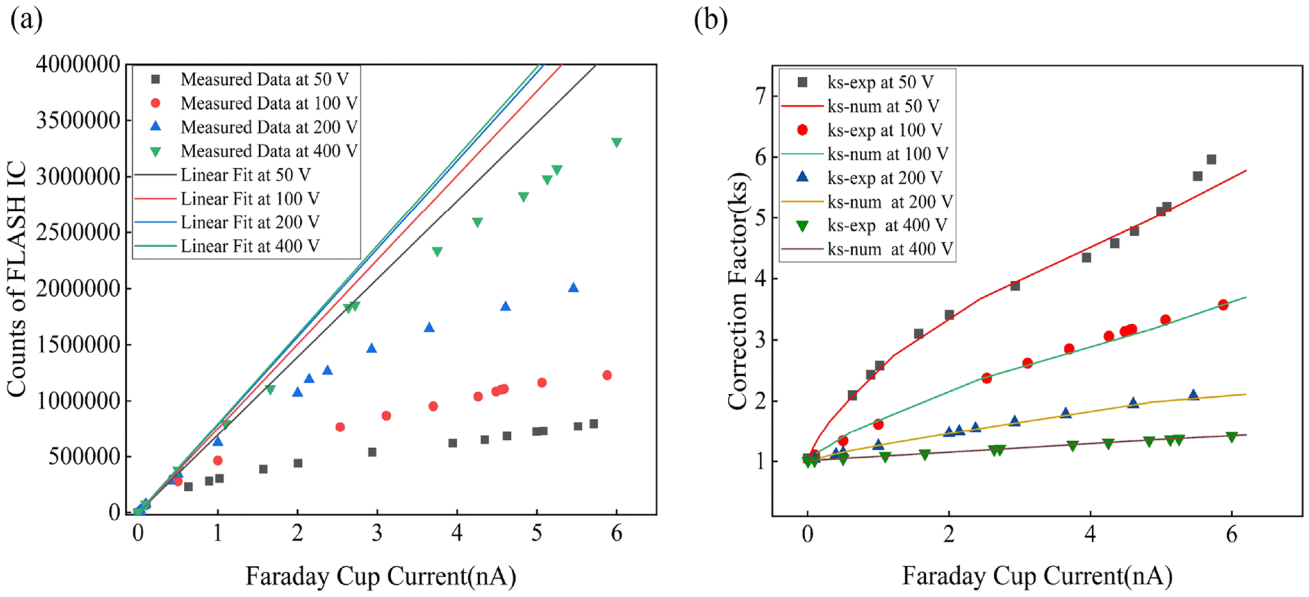

Fig. 6 Figure (**a**) shows the scatter plot of the saturation curve and corrected linear fitting under different applied voltages of IC to change beam current (dose rate). The scatter plot in (**b**) represents the experimental correction factor calculated by Eq. (23), and the curve represents the correction factor calculated by the finite-element model

5 Conclusion

We conducted research on carbon-ion FLASH therapy based on the HIRFL shallow-seated irradiation terminal. A set of beam-monitoring control and dose measurement systems was developed and designed. A finite-element calculation method for the correction factor of the dose saturation curve based on physical phenomenology principles was proposed to realize related research under large-area FLASH IC at an ultra-high dose rate of carbon ions. Considering that the model accuracy of the relevant physical parameters is crucial to the results, its uncertainty leads to significant errors. In the future, we will systematically evaluate and determine physical parameters to reduce model deviation.

In this paper, ideas and methods for dose measurement based on carbon-ion FLASH irradiation are proposed. However, further experimental verification is required to study the biological mechanisms related to FLASH RT, including the effects of different radiation qualities, beam pulse structures, and other factors. Many unsolved problems remain in the field of FLASH. The experimental platform needs to be improved to obtain a higher and more stable average dose rate and to accurately adjust the different durations and repetition frequencies to provide more parameter studies for clinical trials of FLASH to better promote the clinical transformation of FLASH RT.

Acknowledgements We thank the HIRFL-TR4 experimental operators for their support. In addition, we thank our colleagues at the Medical Detection Technology Group of the Institute of Modern Physics, Chinese Academy of Sciences, for their help with the experiments.

Author Contributions All authors contributed to the conception and design of this study. The algorithm proposal and verification, raw data, and analysis were performed by Xin-Le Lang, Zheng-Guo Hu, Zhi-Guo Xu, Juan Li, Kai Zhou, Fa-Ming Luo, Yu-Cong Chen, Li-Bin Zhou, and Guo-Qing Xiao. The first draft of the manuscript was written by Xin-Le Lang, Rui-Shi Mao, Chuan Huang, Zu-Long Zhao, and Jia-Li Fu. All authors commented on previous versions of the manuscript. All authors have read and approved the final version of this manuscript.

Data Availability Statement The data that support the findings of this study are openly available in Science Data Bank at https://cstr.cn/31253.11.sciencedb.j00186.00709 and https://www.doi.org/10.57760/sciencedb.j00186.00709.

Declarations

Conflict of interest The authors declare that they have no conflict of interest.

References

1. Y. Shi, M.Z. Zhang, L.H. Ou-Yang et al., Design of a rapid-cycling synchrotron for flash proton therapy. Nucl. Sci. Tech. **34**, 145 (2023). https://doi.org/10.1007/s41365-023-01283-3
2. W. Zhao, Y. Tian, H. Peng, FLASH radiotherapy. Chin. J. Rad. Oncol. **28**, 11 (2019). https://doi.org/10.3760/cma.j.issn.1004-4221.2019.11.014
3. N. Esplen, L. Egoriti, T. Planche et al., Dosimetric characterization of a novel UHDR megavoltage X-ray source for FLASH radiobiological experiments. Sci. Rep. **14**, 822 (2024). https://doi.org/10.1038/s41598-023-50412-w
4. V. Favaudon, L. Caplier, V. Monceau et al., Ultrahigh dose-rate FLASH irradiation increases the differential response between normal and tumor tissue in mice. Sci. Transl. Med. **6**, 245 (2014). https://doi.org/10.1126/scitranslmed.aba4525
5. Y. Yang, J. Wang, F. Gao et al., FLASH radiotherapy using high-energy X-rays: current status of PARTER platform in FLASH research. Radioth Oncol. **190**, 109967 (2024). https://doi.org/10.1016/j.radonc.2023.109967
6. F. Gao, Y. Yang, H. Zhu et al., First demonstration of the FLASH effect with ultrahigh dose rate high-energy X-rays. Rad. Oncol. **166**, 44–55 (2022). https://doi.org/10.1016/j.radonc.2021.11.004
7. X.Y. Song, Y.P. Song, J. Li et al., Clinical application of proton therapy technology. Chin. Med. Devices (2022). https://doi.org/10.3969/j.issn.1674-1633.2022.03.037
8. S.Y. Wei, C.Y. Shi, C.C. Chen et al., Recent progress in pencil beam scanning FLASH proton therapy: a narrative review. Therap. Radiol. Oncol. **6**, 16 (2022). https://doi.org/10.48550/arXiv.2206.11722
9. Z.Y. Mei, Y. Yuan, J. Wang et al., Focused proton beam generating pseudo Bragg peak for FLASH therapy. Nucl. Instrum. Meth. Phys. Res. A **1032**, 166618 (2022). https://doi.org/10.1016/j.nima.2022.166618
10. W.C. Fang, X.X. Huang, J.H. Tan et al., Proton linac-based therapy facility for ultra-high dose rate (FLASH) treatment. Nucl. Sci. Tech. **32**, 34 (2021). https://doi.org/10.1007/s41365-021-00872-4
11. T.J. Zhang, H.J. Yao, Z.G. Yin et al., Research progress on several aspects of advanced high intensity cyclotron technology at CIAE. Atom. Energy Sci. Technol. **43**, 129–146 (2009). (**in Chinese**)
12. S.Z. An, F.P. Guan, S.M. Wei et al., Development and application of compact high-current proton cyclotron at China Institute of Atomic Energy. Atom. Energy Sci. Technol. **58**, 465–474 (2024). https://doi.org/10.7538/yzk.2024.youxian.0514 (**in Chinese**)
13. H.F. Hao, H.W. Zhao, Q.G. Yao et al., Design of the extraction system of heavy ion medical cyclotron. High Power Laser and Particle Beams. **11**, 2911–2994 (2013). https://doi.org/10.3788/HPLPB20132511.2991
14. R. Liu, Q. Miao, G.X. Shi et al., Development and application of the first carbon ion therapy system in China. Chin. J. Med. Inst. **46**, 517–522 (2022). https://doi.org/10.3969/j.issn.1671-7104.2022.05.009
15. M. Li, W.L. Li, X.C. Kang et al., Radial probe detector system in the cyclotron of heavy ion medical machine. High Power Laser and Particle Beams **35**, 104004 (2023). https://doi.org/10.11884/HPLPB202335.220311
16. Q.K. Duan, G.F. Ding, L.M. Guo et al., Development of FLASH radiotherapy and its application in cancer therapy. Chin. Cancer **31**, 924–928 (2022). https://doi.org/10.11735/j.issn.1004-0242.2022.11.A012
17. J.C. Yang, J. Shi, W.P. Chai et al., Design of a compact structure cancer therapy synchrotron. Nucl. Instrum. Meth. Phys. Res. A **756**, 19–22 (2014). https://doi.org/10.1016/j.nima.2014.04.050
18. M. Durante, E. Bräuer-Krisch, M. Hill, Faster and safer? FLASH ultra-high dose rate in radiotherapy. The Brit. J. Radiol. **1082**, 91 (2018). https://doi.org/10.1259/bjr.20170628
19. Y.L. Yi, M.G. Stabin, The effects of abnormal exposure on individual dose monitoring with TLD dosimeter. Health Phys. **127**, 730–733 (2024). https://doi.org/10.1097/HP.0000000000001874
20. S.W. Yang, S.K. Park, C.W. Moon et al., Development of a hybrid line dosimeter using lead (II) iodide and GdOS: Tb for dose

monitoring in brachytherapy. J. Instrum. **18**, 9 (2023). https://doi.org/10.1088/1748-0221/18/09/P09042
21. L. Schoenauen, R. Coos, J.L. Colaux et al., Design and optimization of a dedicated Faraday cup for UHDR proton dosimetry: implementation in a UHDR irradiation station. Nucl. Instrum. Meth. Phys. Res. A **1064**, 169411 (2024). https://doi.org/10.1016/j.nima.2024.169411
22. P. Andreo, D.T. Burns, K. Hohlfeld, et al., Absorbed dose determination in external beam radiotherapy: An international code of practice for dosimetry based on standards of absorbed dose to water. IAEA (2000)
23. P.R. Almond, P.J. Biggs, B.M. Coursey et al., AAPM's TG-51 protocol for clinical reference dosimetry of high-energy photon and electron beams. Med. Phys. **9**, 26 (1999). https://doi.org/10.1118/1.598691
24. F. Gómez, D.M. Gonzalez-Castaño, N.G. Fernández et al., Development of an ultra-thin parallel plate ionization chamber for dosimetry in FLASH radiotherapy. Med. Phys. **49**, 4705–4714 (2022)
25. L.S. Yin, W. Zou et al., Evaluation of two-voltage and three-voltage linear methods for deriving ion recombination correction factors in proton FLASH irradiation. IEEE T. Radiat. Plas. Med. Sci. **6**, 263–270 (2022). https://doi.org/10.1109/TRPMS.2021.3078885
26. J.W. Boag, Ionization measurements at very high intensities. British J. Radiol. **274**, 601–611 (1952). https://doi.org/10.1259/0007-1285-23-274-601
27. J.W. Boag, E. Hochhäuser, O.A. Balk, The effect of free-electron collection on the recombination correction to ionization measurements of pulsed radiation. Phys. Med. Biol. **5**, 41 (1996). https://doi.org/10.1088/0031-9155/41/5/005
28. S.J.J. Thomson, G.P. Thomson, Conduction of electricity through gases
29. I. Langmuir, Kinetic theory and electric conduction through gases. Nature **123**, 675–676 (1929). https://doi.org/10.1038/123675a0
30. M. Gotz, L. Karsch, J. Pawelke, A new model for volume recombination in plane-parallel chambers in pulsed fields of high dose-per-pulse. Phys. Med. Biol. **22**, 62 (2017). https://doi.org/10.1088/1361-6560/aa8985
31. Q. Li, Z. Dai, Z. Yan et al., Heavy-ion conformal irradiation in the shallow-seated tumor therapy terminal at HIRFL. Med. Biol. Eng. Comp. **11**, 45 (2007). https://doi.org/10.1007/s11517-007-0245-3
32. R. He, X.-Y. Niu, Y. Wang et al., Advances in nuclear detection and readout techniques. Nucl. Sci. Tech. **34**, 205 (2023). https://doi.org/10.1007/s41365-023-01359-0
33. X. Lang, Z. Hu, Z. Zhao et al., Preliminary study of low-pressure ionization chamber for online dose monitoring in FLASH carbon ion radiotherapy. Phys. Med. Biol. **2**, 69 (2024). https://doi.org/10.1088/1361-6560/ad13d0
34. U.A. Weber, E. Scifoni, M. Durante, FLASH radiotherapy with carbon ion beams. Med. Phys. **3**, 49 (2022). https://doi.org/10.1002/mp.15135
35. F.A. Cucinotta, H. Nikjoo, D.T. Goodhead, Applications of amorphous track models in radiation biology. Radiat. Environ. Biophys. **2**, 38 (1999). https://doi.org/10.1007/s004110050142
36. Hundsdorfer. Numerical Solution of Time-Dependent Advection-Diffusion-Reaction (2003)
37. E.W. McDaniel, Gray EP. Collision phenomena in ionized gases. (1964)
38. Smoluchowski MJAdP. Zur kinetischen Theorie der Brownschen Molekularbewegung und der Suspensionen. 326 (1906)
39. Einstein AJAdP. Über die von der molekularkinetischen Theorie der Wärme geforderte Bewegung von in ruhenden Flüssigkeiten suspendierten Teilchen. **17**, 549 (1905)
40. E. Hochhaeuser, O.A. Balk, H. Schneider et al., The significance of the lifetime and collection time of free electrons for the recombination correction in the ionometric dosimetry of pulsed radiation. J. Phys. D Appl. Phys. **27**, 431 (1994). https://doi.org/10.1088/0022-3727/27/3/001
41. G.B. Chambres, d'ionisation en Protonthérapie et hadrontherapie Dissertation Normandy Université Caen. (2015)
42. T. Kanai, M. Sudo, N. Matsufuji et al., Initial recombination in a parallel-plate ionization chamber exposed to heavy ions. Phys. Med. Biol. **12**, 43 (1998). https://doi.org/10.1088/0031-9155/43/12/012
43. M. Zauner-Wieczorek, J. Curtius, A. Kürten, The ion-ion recombination coefficient α: comparison of temperature- and pressure-dependent parameterisations for the troposphere and stratosphere. Atmos. Chem. Phys. **18**, 22 (2022). https://doi.org/10.5194/acp-22-12443-2022